REPORT SM-49105-F4

STRESS CORROSION CRACKING OF TITANIUM ALLOYS AT AMBIENT TEMPERATURE IN AQUEOUS SOLUTIONS

Yearly Summary Report
September 1969 to September 1970
Under Contract NAS7-488

MCDONNELL DOUGLAS ASTRONAUTICS COMPANY

MCDONNELL DOUGLAS CORPORATION

SEPTEMBER 1970

Report SM-49105-F4

STRESS CORROSION CRACKING OF TITANIUM ALLOYS AT AMBIENT TEMPERATURE IN AQUEOUS SOLUTIONS

Yearly Summary Report
for Sept. 1969 to Sept. 1970

Contract NAS 7-488

Administered by
Chief, Research SRT NASA Headquarters
Code RRM

Prepared by:

T. L. Mackay, Ph. D.
Materials Research and Development Specialist

ASTROPOWER LABORATORY
McDonnell Douglas Astronautics Company — West
Newport Beach, California

FOREWORD

This report was prepared by Astropower Laboratory, McDonnell Douglas Astronautics Company--West, under NASA Contract NAS 7-488. It is a yearly summary report and covers work conducted from September 1969 to September 1970. The work is administered by Chief, Research SRT, NASA Headquarters, Code RRM, with Mr. Richard M. Raring as Project Scientist.

Principal Investigator on the program is Dr. T. L. Mackay of Astropower Laboratory. Dr. S. K. Asunmaa and R. Ingersoll contributed greatly with the electron microscopy.

ABSTRACT

The effect of aluminum concentrations on the stress corrosion susceptibility of α-titanium in aqueous 3-percent NaCl salt environments at ambient temperature was studied. Five experimental alloys with aluminum concentrations from 5.0 to 7.0 weight percent were tested in equiaxed and quenched α-phase microstructures. Susceptibility to stress corrosion cracking was found to increase very rapidly above 5.5 weight percent Al. Transmission electron microcopy studies were conducted to measure the stacking energies of titanium-aluminum alloys containing 5.0 to 8.5 weight percent Al. The most reliable measurement was obtained with the highest aluminum alloy, Ti-8.5 weight percent Al, which had a stacking fault energy of 9.9 ± 0.5 erg/cm^2. It is postulated that the coplanar prism slip observed with increasing aluminum concentration is primarily responsible for stress-corrosion crack initiation, while decreasing stack fault energy with increasing aluminum concentration would explain the basal- or near basal-plane cleavage observed in stress corrosion cracking of alpha and alpha-beta titanium alloys.

An analysis was made of the effect of a stress field at 450°F and 600°F precipitation of hydrides in pure titanium containing 0.76 percent hydrogen. Two possibilities that would explain the presence of large precipitates in pure titanium with the hydrogen content considerably below the solubility limit were considered:

A. The effect of pressure on $\alpha/\alpha+\gamma$ phase boundary in Ti-H.
B. The effect of defect structure introduced by creep processes.

The estimated shift in the solubility equilibrium curve was found to be negligible and clearly indicates that the large gamma hydride precipitates observed in α-titanium did not occur during the stressing cycle. It seems logical to assume that the dislocations introduced into the α-titanium during the stressing cycle served as nucleation sites for gamma hydride precipitates during the quenching cycle. It was found that the habit plane of gamma hydride precipitates was predominately $\{10\bar{1}0\}$.

CONTENTS

FIGURES

TABLES

1.0 INTRODUCTION AND SUMMARY

Astropower Laboratory has been engaged in a NASA-sponsored research program to develop fundamental knowledge about the mechanism of stress corrosion cracking (SCC) of titanium alloys in aqueous solutions. Study of the behavior of alpha and alpha-beta alloys was emphasized because of their known susceptibility to SCC. Both alloys are used for propellant tankage materials as well as for aircraft transport applications that require a high degree of structural reliability with negligible probability of sudden failure.

Results obtained on this investigation, prior to the current year, have been presented in detail in Yearly Summary Reports SM-49105-F1, SM-49105-F2 and SM-49105-F3.

Studies during the current contract year include:

A. Investigate the influence of aluminum concentration on the stress corrosion susceptibility of α-titanium at ambient temperature.

B. Measure the stacking fault energy of binary α-titanium alloys as a function of aluminum content and relate this to SCC susceptibility.

C. Investigate the effects of stress and temperature on hydrogen diffusion and hydride precipitation in alpha and in alpha-beta titanium alloys to define the role of hydrogen embrittlement.

The effect of aluminum concentration on the stress corrosion susceptibility of α-titanium in aqueous 3-percent NaCl salt solution was studied. Stress corrosion tests using partial-through-crack specimens showed susceptibility increases very rapidly above 5.5 weight percent aluminum. Even in the concentration range of 5.0 to 5.5 weight percent Al, complete immunity to stress corrosion cracking was not observed.

The dislocation arrangement in deformed titanium-aluminum alloys changes from dislocation tangles in Ti-4.5 weight percent Al to planar groupings in alloys containing higher Al. Studies were initiated to measure the stacking fault energies of titanium-aluminum containing 5.0 to 8.5 weight percent Al. The most reliable measurements were considered to be obtained with Ti-8.5 weight percent Al. For this alloy a value of

9.9 ± 0.5 erg/cm^2 was obtained. The stacking fault measured was for the reaction

$$\frac{a}{3}[2\bar{1}\bar{1}0] = \frac{a}{3}[1\bar{1}00] + \frac{a}{3}[10\bar{1}0].$$

More precise measurements are needed to show the effect of aluminum concentration on stacking fault energy in α-titanium.

An analysis was made of the effect of a stress field at 450°F and 600°F precipitation of hydrides in pure titanium containing 0.76 percent hydrogen. Two possibilities that would explain the pressure of large precipitates in pure titanium with the hydrogen content considerably below the solubility limit were considered:

A. The effect of pressure on $\alpha/\alpha+\gamma$ phase boundary in Ti-H.

B. The effect of defect structure introduced by creep processes.

The estimated shift in the solubility equilibrium curve was found to be negligible and clearly indicated that the large gamma hydride precipitates observed in α-titanium did not occur during the stressing cycle. It seems logical to assume that the dislocations introduced into the α-titanium during the stressing cycle serve as nucleation sites for gamma hydride precipitates during the quenching cycle. It was found that the habit plane of gamma hydride precipitates was predominately $\{10\bar{1}0\}$.

2.0 EXPERIMENTAL EVALUATIONS

2.1 Effect of Aluminum Concentration on Stress Corrosion Susceptibility of α-titanium

The effect of aluminum concentration on the stress corrosion susceptibility of α-titanium in aqueous 3-percent NaCl salt environments at ambient temperature was studied. Five experimental alloys with aluminum concentrations from 5.0 to 7.0 weight percent were tested in equiaxed and quenched α-phase microstructures.

Aluminum plays an important role in the dislocation arrangement in α-titanium. Increasing the aluminum content above 4.5 weight percent Al changes dislocation patterns from dislocation tangles to coplanar arrays.[1] Studies were initiated to measure the stacking fault energies of titanium-aluminum alloys containing 5.0 to 8.5 weight percent Al and to relate this to SCC susceptibility.

2.1.1 Stress Corrosion Cracking of Titanium-Aluminum Alloys

Five experimental titanium-aluminum alloys were vacuum arc cast at Titanium Metals Corp. of American (TMCA) with the following nominal aluminum concentration:

Ti-5.0 Al
Ti-5.5 Al
Ti-6.0 Al
Ti-6.5 Al
Ti-7.0 Al

Eighth-inch sheet material was prepared by the following fabrication sequence: Ingots were forged to 3-inch square form in the temperature range 2100 to 2200°F, cut into 1-1/2 inch thick bars, and rolled to 1/8 by 4 inches in the temperature range 1900 to 2000°F. Figure 1 shows a typical rolled titanium-aluminum sheet. Table I shows the averages of chemical analyses taken from rolled sheet.

Specimens for stress corrosion studies and mechanical properties were taken from the longitudinal direction of rolling. The specimens were vacuum annealed, 10^{-6} torr at 1500°F, for two hours

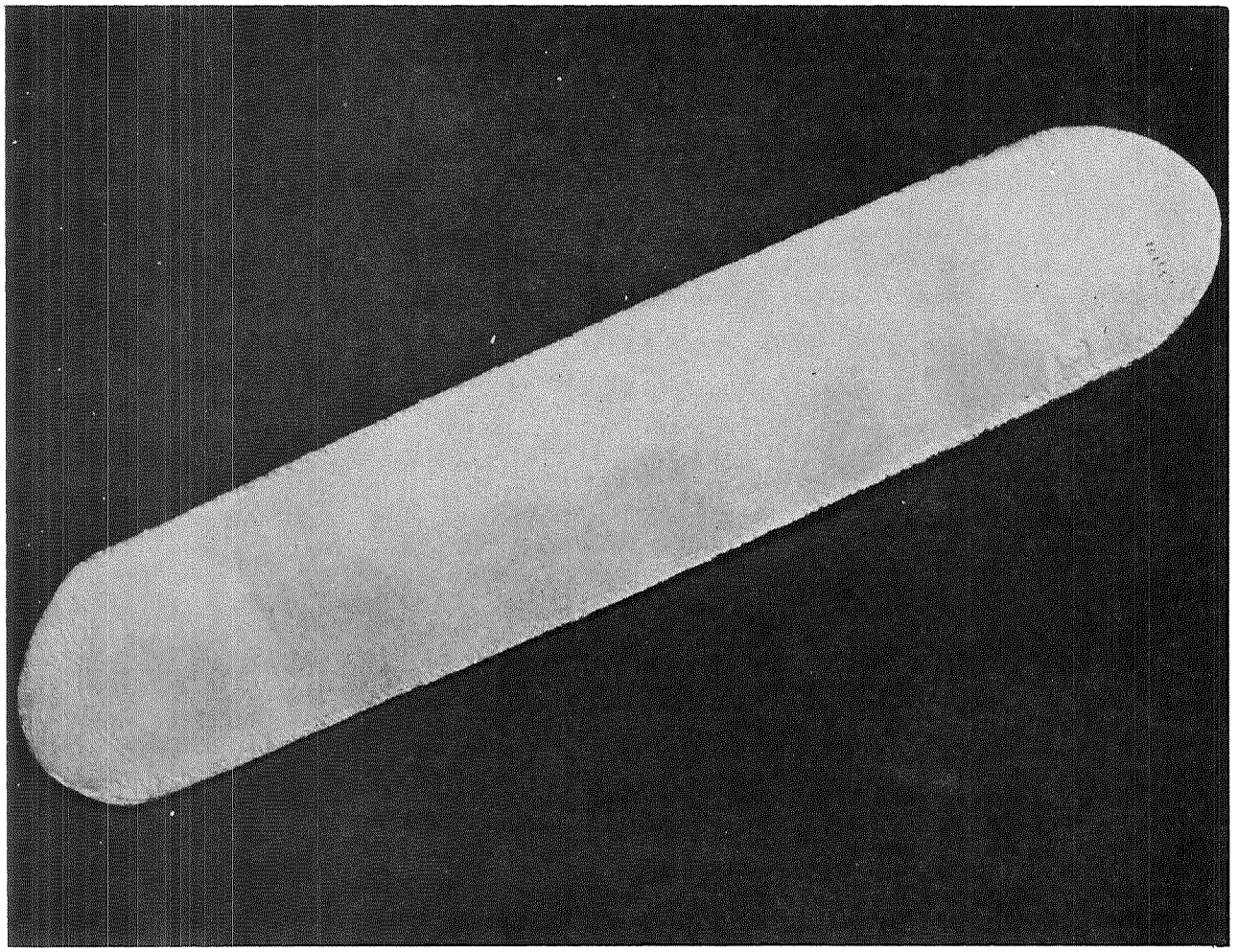

Figure 1. Photograph of 1/8-Inch Rolled Titanium-Aluminum Alloy Sheet from Arc-Cast Ingot

and then water quenched. The mechanical properties of the experimental alloys are shown in Table II.

Stress corrosion cracking experiments were performed using partial-thickness crack (PTC) specimens. Sufficient data exist to show that the determination of plane-strain fracture toughness properties does not depend on gross specimen configuration when a PTC specimen is used, although there are some limitations imposed when the resulting data are to be treated by the linear elastic fracture mechanics. These limitations are that (1) the crack depth should not exceed half the thickness of the material and (2) the area of the shallow crack should be less than 10 percent of the gross cross sectional area of the test specimen.

The effect of crack shape on the critical stress intensity K_{IC} is usually accounted for in calculations using PTC test results by means of the parameter Φ as:

$$K_{IC}^2 = \frac{1.21\pi a\sigma^2}{\Phi^2 - 0.212\left(\frac{\sigma}{\sigma_y}\right)^2} \qquad (1)$$

where

σ = gross fracture stress
σ_y = 0.2 percent yield strength
a = depth of surface crack.

The shape parameter, Φ, is a complete integral as:

$$\Phi = \int_0^{\pi/2}\left[1 - \frac{c^2 - a^2}{2}\sin^2\theta\right]^{1/2} d\theta \qquad (2)$$

where c is the surface half length of the crack. The integral is solvable by an infinite series but is equivalent to the emperical relationship developed at McDonnell Douglas

$$\Phi^2 = 4.593\left(\frac{a}{2c}\right)^{1.650} + 1 \qquad (3)$$

The critical stress intensity describes the effect of flaws on the residual strength of a member at stress levels less than the yield strength. At

Table I

CHEMICAL ANALYSIS OF TITANIUM-ALUMINUM BINARY VACUUM ARC-MELTED INGOTS (PERCENT WEIGHT)

Alloy	Al	Fe	O	N
1	5.21	0.040	0.097	0.006
2	5.50	0.029	0.095	0.005
3	6.12	0.035	0.081	0.004
4	6.46	0.033	0.096	0.005
5	6.73	0.025	0.104	0.003

Table II

MECHANICAL PROPERTIES OF TITANIUM-ALUMINUM ALLOYS

Alloy	0.2 Percent Yield (ksi)	Ultimate Tensile (ksi)	Elastic Modulus ($\times 10^6$)	El (percent)
1	95.5	109.5	19.1	19.0
2	97.8	111.3	20.7	19.0
3	98.3	113.4	19.7	20.0
4	103.2	115.8	19.1	20.0
5	108.5	122.3	21.3	20.0

Average of three specimens.

stresses above the yield strength, the elastic analysis, which forms the basis of the expression for stress intensity, fails to account for the large plastic strains and Equation (1) no longer describes the observed behavior.

The factor 1.21 in Equation (1) is intended to account for the effects on stress intensity of the interference in the stress field caused by the free surface of the member in which the surface crack exists. The actual value of the magnification factor should vary with crack shape and with proximity of the deepest part of the crack to the back surface. For cracks up to about 50 percent of the member thickness in depth, the actual value of the factor is close to 1.1. For cracks deeper than 50 percent of the thickness of the member, however, the factor increases beyond 1.1.[2]

The recommendations of ASTM committee E-24 are that the thickness of a partial-through crack specimen shall be greater than $2.5\left(\frac{K_{IC}}{\sigma ys}\right)^2$. For these experimental titanium - aluminum alloys, this would require thicknesses greater than 1 inch in order to obtain plane strain conditions at room temperature. However, if the artificial flaws introduced meet the following requirements $a_o < \beta/2$, $2C_o \leq \frac{w}{3}$, and $\frac{w}{\beta} > 6$, crack growth will attain critical size under conditions of plane strain for plates with thicknesses less than those specified by committee E-24. The surface cracked specimen configuration used for stress corrosion cracking experiments is based on the above requirements and is shown in Figure 2. Semielliptically shaped surface flaws with approximate dimensions of $2c = 0.25$ inch and $a_o = 0.050$ inch were made by a discharge machine and low stress fatigue.

The initial stress intensity factor, K_{Ii}, was measured using the load sustained in the test and the initial crack dimensions. Values of initial stress intensity factor, K_{Ii}, measured in 3-percent salt solution (NaCl) at ambient temperature with values obtained in air are shown in Table III for the five experimental alloys. Figure 3 shows the initial stress intensity factor, K_{Ii}, for the five experimental alloys in 3-percent NaCl solution as a function of time-to-failure and the sustained load tests in air at ambient temperature for the titanium alloy, 5.5 weight percent Al.

Titanium alloys 3 and 4 with aluminum concentrations ranging from 6.1 to 6.75 weight percent were found to be very sensitive to stress corrosion cracking at ambient temperature in 3-percent

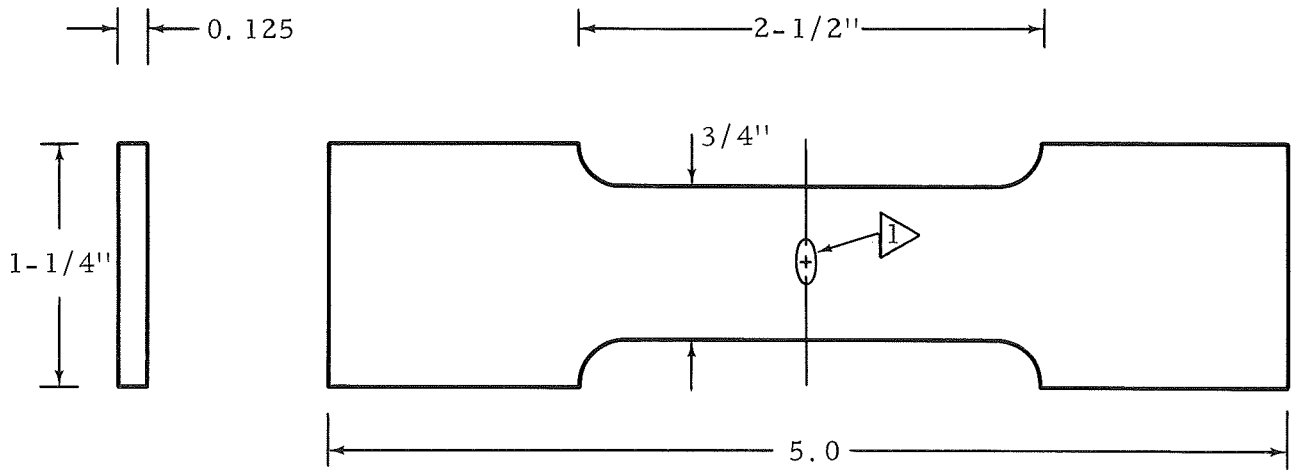

1 Semiellipitcally Shaped Flaw Made by Discharge Machine and Low Stress Fatigue

Figure 2. Surface-Flawed Specimen for 0.125-Inch Titanium-Aluminum Alloys at Ambient Temperature

Table III

EFFECT OF ALUMINUM CONTENT ON STRESS CORROSION OF α-TITANIUM IN 3-PERCENT NaCl

Specimen Number	Al	Environment	K_{Ii} ksi$\sqrt{in}$	Time to Fracture
1-1	5.2	Air	40.5	-
1-2	5.2	Air	37.0	2 min
1-3	5.2	3 Percent NaCl	36.6	2 min
1-4	5.2	3 Percent NaCl	35.7	8.5 min
1-5	5.2	3 Percent NaCl	35.1	25 min
1-6	5.2	3 Percent NaCl	34.0	2 hr*
2-1	5.5	Air	38.0	-
2-2	5.5	Air	40.0	6 min
2-3	5.5	Air	35.0	50 min
2-4	5.5	Air	34.3	2.8 hr
2-5	5.5	Air	33.9	100 hr*
2-6	5.5	3 Percent NaCl	40.0	15 sec
2-7	5.5	3 Percent NaCl	36.6	30 sec
2-8	5.5	3 Percent NaCl	35.0	30 sec
2-9	5.5	3 Percent NaCl	34.6	2 min
2-10	5.5	3 Percent NaCl	34.0	72 min
2-11	5.5	3 Percent NaCl	33.5	4.7 hr
2-12	5.5	3 Percent NaCl	33.2	72.4 hr
2-13	5.5	3 Percent NaCl	32.7	100 hr*
3-1	6.1	Air	40.0	
3-2	6.1	3 Percent NaCl	28.7	12.5 min
3-3	6.1	3 Percent NaCl	27.1	65 min
3-4	6.1	3 Percent NaCl	23.8	150 min
3-5	6.1	3 Percent NaCl	23.5	75 hr*
4-1	6.5	Air	41.8	
4-2	6.5	3 Percent NaCl	26.4	33 min
4-3	6.5	3 Percent NaCl	23.3	11 min
4-4	6.5	3 Percent NaCl	22.5	72 min
5-1	6.75	3 Percent NaCl	41.7	-
5-2	6.75	3 Percent NaCl	30.4	30 sec
5-3	6.75	3 Percent NaCl	29.0	1.0 min
5-4	6.75	3 Percent NaCl	26.5	2.0 min
5-5	6.75	3 Percent NaCl	25.0	3.0 min
5-6	6.75	3 Percent NaCl	21.7	50 min*
5-7	6.75	3 Percent NaCl	21.1	80 hr

*No failure.

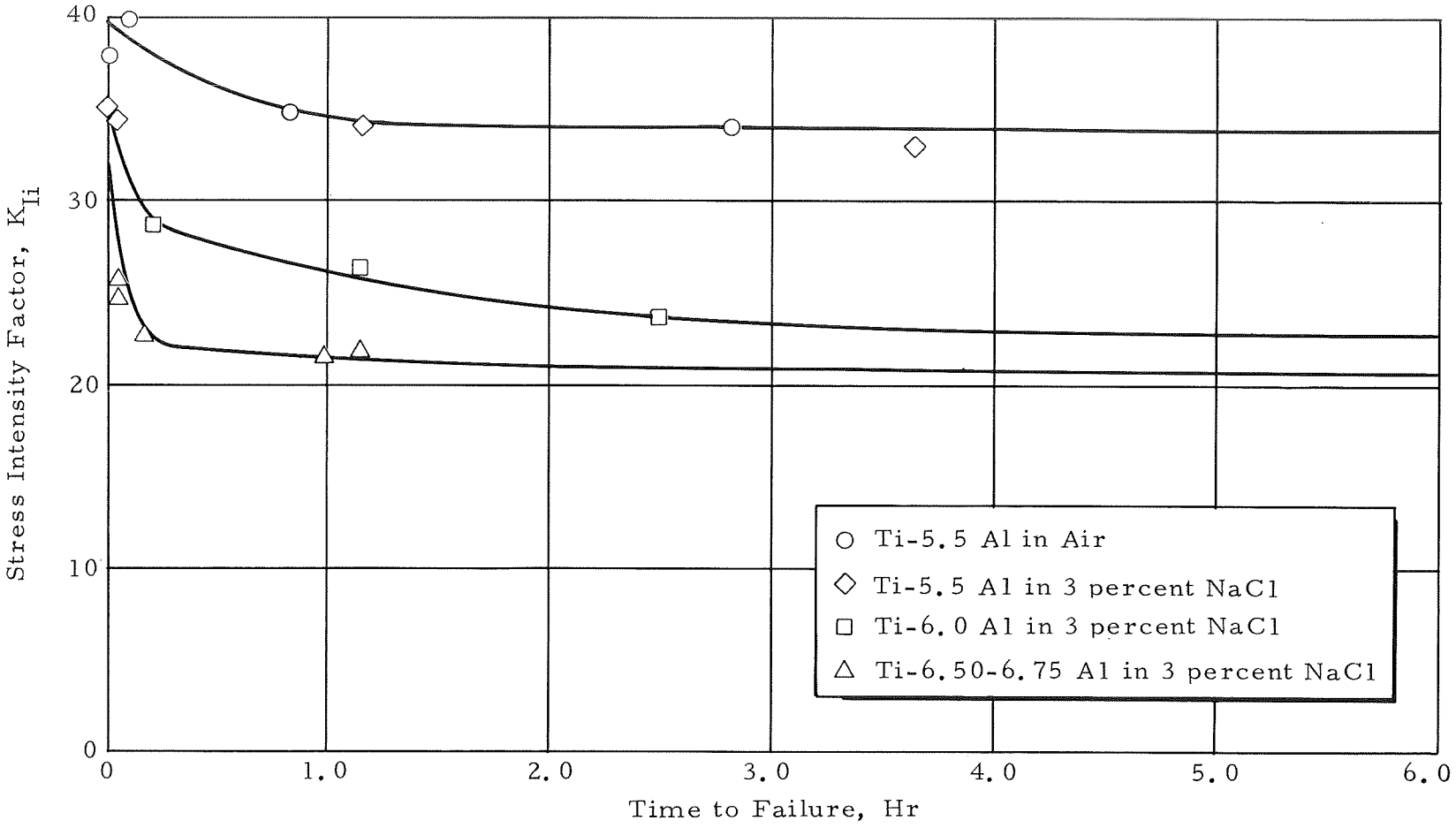

Figure 3. Effect of Initial Stress Intensity on Time-to-Fracture for Titanium-Aluminum Alloys in 3-percent NaCl at Ambient Temperature

NaCl. Titanium alloys 1 and 2 containing 5.2 to 5.5 weight percent Al were found to be considerably less susceptible to stress corrosion cracking than alloys 3, 4 and 5.

From these sustained load tests, it is evident that aluminum concentration increases susceptibility to SCC in α-titanium very rapidly above 5.5 weight percent Al. Even in the concentration range 5.0 to 5.5 weight percent Al, complete immunity to stress corrosion cracking was not observed. When the stress intensity factor was increased above 34 ksi $\sqrt{\text{in.}}$, the time-to-failure was reduced considerably in 3-percent NaCl solution for these two alloys. Figures 4 and 5 are electron fractographs of specimens 2-3 and 2-8, which were fractured at 35.0 ksi $\sqrt{\text{in.}}$ in air and 3-percent NaCl respectively. In Figure 4, a ductile microstructure is observed at a crack origin in a specimen fractured in air, whereas brittle cleavage is observed at the crack origin in a specimen fractured in 3-percent NaCl.

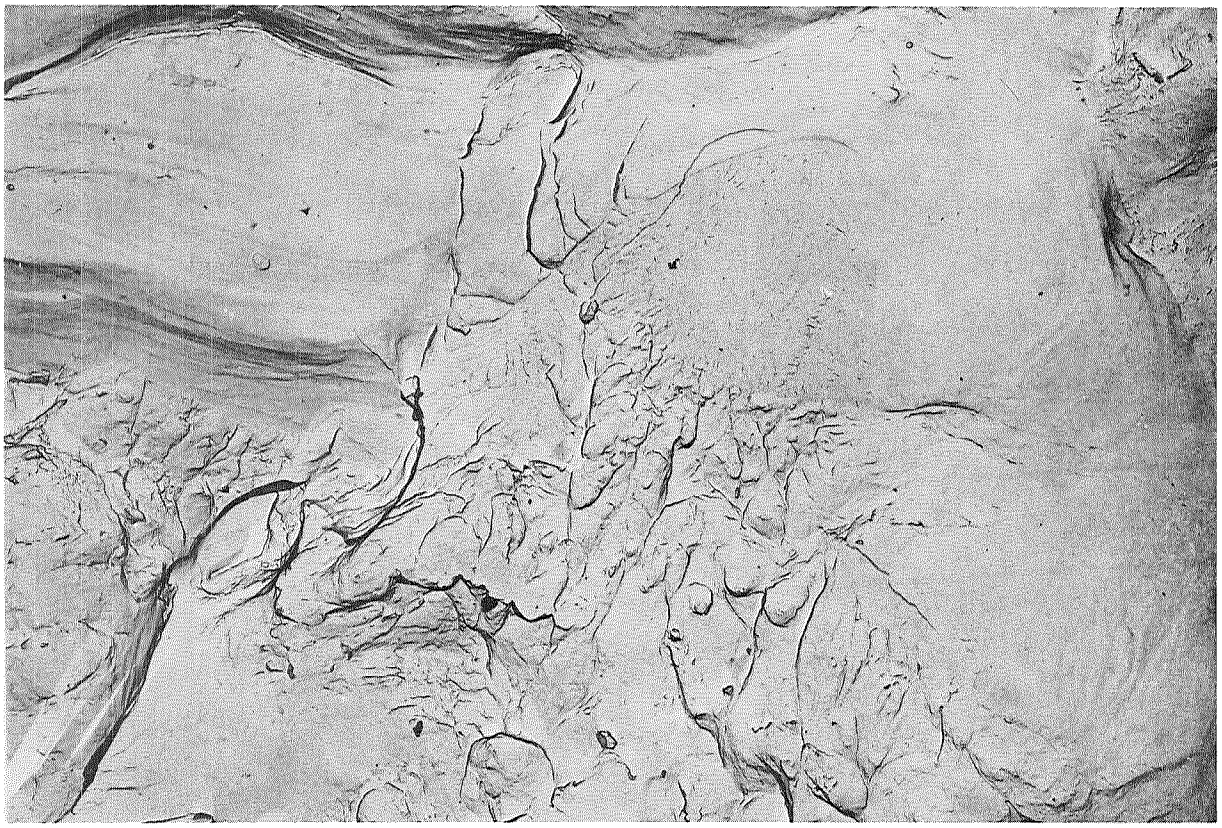

Figure 4. Electron Fractograph of Ti-5.5 Weight Percent Al Fractured in Air Showing Ductile Failure (Magnification 7,500X)

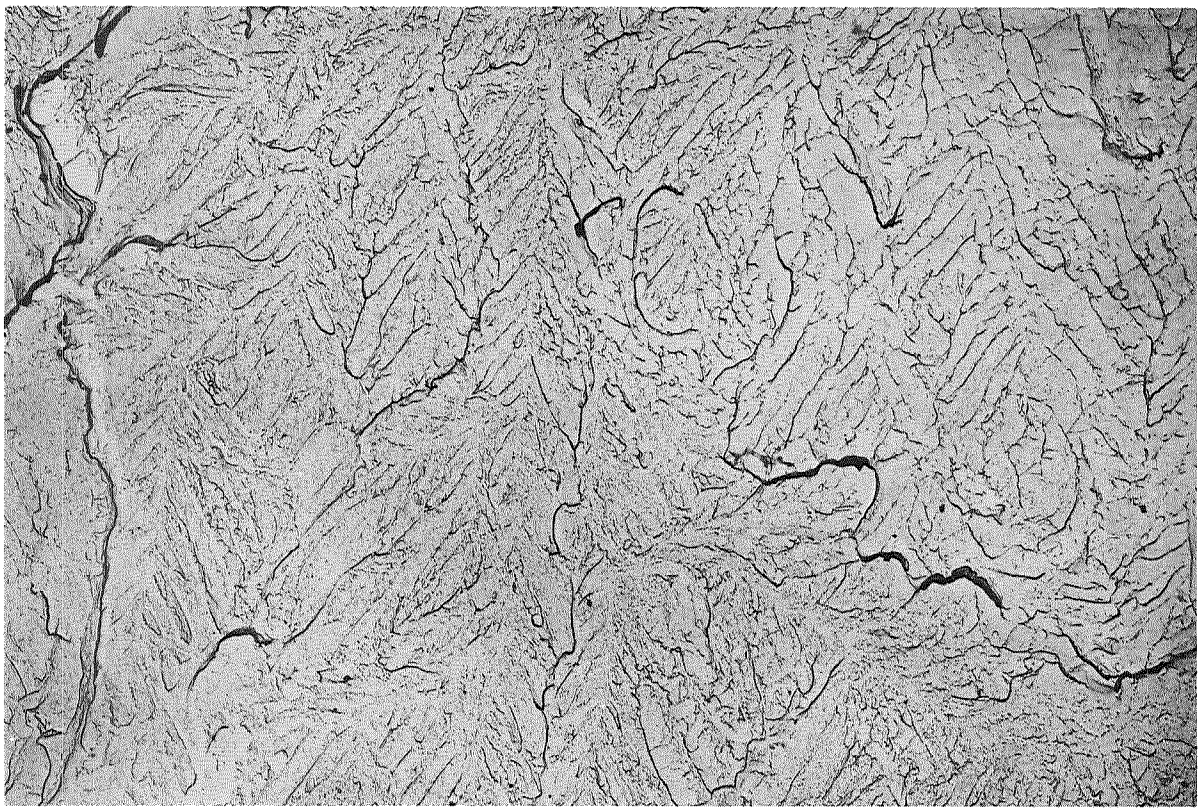

Figure 5. Electron Fractograph of Stress Corrosion Region of Ti-5.5 Weight Percent Al Fractured in 3-percent Salt Solution Showing Cleavage Failure (Magnification 7,500X)

2.1.2 Stacking Fault Energies in Ti-Al Alloys

The dislocation arrangement in deformed α-titanium alloys changes from dislocation tangles in Ti-4.5 weight percent Al to planar groupings predominately on prism planes,[3] in alloys containing more aluminum. Since aluminum may have an influence on the stacking fault energy (SFE), a study of SFE and dislocation interaction of α-titanium alloys was initiated. An attempt will be made to correlate these results with stress corrosion susceptibility.

There are several methods of estimating stacking fault energies in metals. These include methods employing the measurement of material properties (such as the strain rate dependence of τ_3, the textures produced by deformation, and the measurement of X-ray peak shifts) and methods that measure defect parameters by direct observation of defects (such as extended dislocation nodes, dislocation double ribbons, and the shrinkage rate of faulted and unfaulted dislocation loops). Gallagher and Liu[4] have compared the accuracy of the different methods and have concluded that the most reliable techniques are those that measure the defect directly.

The measurement of dislocation nodes was used in this investigation. There are three methods[5, 6, 7] for calculating SFE from dislocation nodes now being used. Gallagher[8] has shown that the methods Brown and Tholen [5] and Siems [6] agree very closely and probably give better results than that of Jossang et al.[7] For these reasons, only the method of Brown and Tholen was used for calculating stacking fault energy. The expression for calculating stacking fault energies, according to Brown and Tholen, is as follows:

$$\gamma = \frac{Gb^2}{\omega}\left[0.055\left(\frac{2-\nu}{1-\nu}\right) - 0.06\left(\frac{\nu}{1-\nu^2}\right)\cos 2\alpha + \left\{0.018\left(\frac{2\nu}{1-\nu}\right) + 0.36\left(\frac{\nu}{1-\nu}\right)\cos 2\alpha\right\}\log\frac{\rho}{\varepsilon}\right] \quad (4)$$

where

γ = the stacking fault energy in erg/cm^2

ω = the inscribed radius in cm

b = the Burger's vector of the partial dislocation element

ν = Poisson's ratio

α = the angle between b and the tangent to dislocation element. $\alpha = 0°$ for screw nodes and 90° for edge nodes.

ρ = the radius of curvature of the node

ε = the cutoff radius

There has been little effort to date to measure the stacking fault energy of hexagonal close packed metals and alloys. Ericsson[9] measured the SFE of two Ni-Co alloys, Ashee and Vassamillet[10] a Cu-Ga alloy, and Ruff and Ives[11] a series of Ag-Zn alloys. The stacking fault energy has been for the reaction

$$\frac{a}{3}[2\,\bar{1}\,\bar{1}\,0] = \frac{a}{3}[1\,\bar{1}\,0\,0] + \frac{a}{3}[1\,0\,\bar{1}\,0] \qquad (5)$$

This reaction is caused by dislocations in the basal plane dissociating into Shockley partials, which reduces their energy. Their reaction is applicable to the Ti-Al alloys being considered.

When photographing nodes for calculating SFE, low order Bragg reflections should be chosen in order to keep the dislocation width to a minimum; as higher order reflections are used, the dislocation width becomes wider, causing more error in measuring the node. The width has been given by Whelan[12] as t_o/π where t_o is the extinction distance for a given Bragg reflection. For the dislocation reaction shown above, Ruff and Ives[11] have shown that the $[2\,\bar{2}\,0\,0]$ and $[\bar{2}\,1\,1\,0]$ reflections are desirable since the former shows stacking fault contrast and the latter shows dislocation line contrast. Furthermore, the partial dislocation Burger's vectors $\vec{b}p$ with the $[2\,\bar{2}\,0\,0]$ reflection ($\vec{g}$) give $|n| = \vec{g} \cdot \vec{b} = 2/3$ or $4/3$, which is sharp enough for good measurement. Unfortunately, the Siemens Elmiskop I microscope used for this study did not have a tilting stage so that the $\vec{g}$ reflection could not be controlled. Therefore, it was not possible to examine $\vec{g}$ in stacking fault contrast and dislocation line contrast. Without this ability the results obtained are much less accurate.

Most of the nodes were photographed at 20,000X and enlarged to 100,000X or 350,000X. These prints were then measured under a 7-power stereo microscope. The inscribed radius (ω) was obtained by fitting standard size circles in the node. It was not necessary to correct the measured (ω) for tilting of the node, since all transmission electron-micrographs were taken close to the basal plane. Figure 6 shows a typical symmetrical dislocation node examined in this investigation. The dislocation width (d) was also measured.

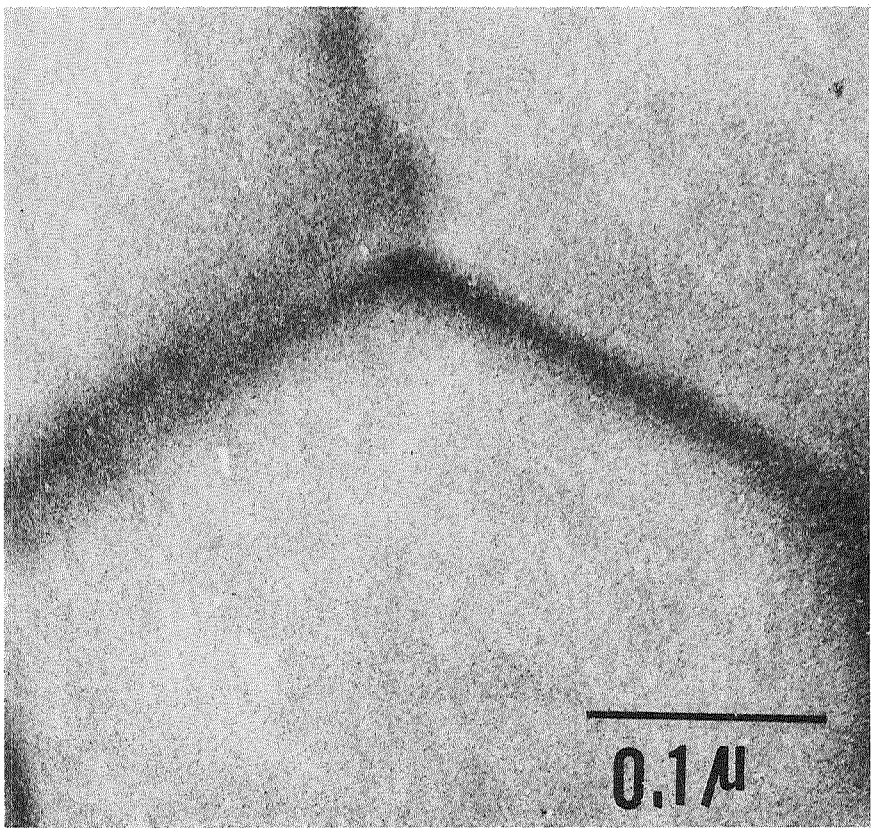

Figure 6. Example of Extended Dislocation Node in Titanium Alloy, Ti-8.5Al

For this investigation the following values were used in Equation (4) to calculate stacking fault energy: G = 4.8 x 10 in. dyne/cm^2. This was not measured for these alloys so the value for the alloy, Ti-5Al-2.5Zn, was selected. ν = 0.31 ε = b = 1.696. Pearson[13] gives the effect of Al on the lattice parameters of Ti-Al alloys. For the alloys being studied a value of a = 2.935 was chosen and b = $a/\sqrt{3}$ = 1.696. Theoretical considerations give ε = b or b/2 or b/4; the effect of choosing ε = b has been discussed by others [4, 7]. This change of a factor of 4 caused a 20 percent variation in Gallagher's[8] SFE; however, Gallagher, as do all other investigators, chose ε = b for his reported values of γ, α = 10 degrees. Prism slip bands were available in most foils and an estimate could be made. This value averaged 10 degrees. This angle is somewhat closer to the screw orientation than Ruff and Ives report for Ag-Zn alloys where they found a preference for angles between 10 and 30 degrees, ρ/ω = 4.44 for α = 0 and 2.90 for α = 90 degrees. Brown and Tholen[5] give a theoretical calculation of ρ/ω as a function of α. The careful experiments of Gallagher[8] show that the measured ρ/ω is close to the theoretical. Since it is much more difficult to measure ρ than ω, the theoretical values of ρ/ω were used to calculate ρ from the experimental measurement of ω.

Results of calculations assuming screw dislocations are shown in Table IV. The large variation in the measured values of ω is usual[9]. Therefore, the data were treated statistically by calculating the standard deviation ($\bar{s}$)

$$\bar{s} = \sqrt{\frac{\sum(\omega i - \bar{\omega})^2}{N(N-1)}} \qquad (6)$$

where ωi is measured value of ω for the node i. $\bar{\omega}$ is the mean value of measured ω. N is tht total number of nodes measured.

This standard deviation was then used to calculate the change in stacking fault energy ($\Delta\gamma$) when $\bar{s}$ is added or subtracted from the mean radius ω. The most reliable measurements shown in Table IV were obtained with the highest aluminum alloy, Ti-8.5 Al, which had a stacking fault energy of 9.9 ± 0.5 erg/cm^2. The ratio ω/d was about 2.2 for the Ti-8.5 Al alloy, which according to Gallagher, [8] should provide reliable SFE. More precise measurements of stacking fault energies are needed however at the lower aluminum concentrations.

Table IV

CALCULATION RESULTS ASSUMING SCREW DISLOCATIONS

Material	Number of Nodes	ω mean Å	ω max Å	ω min Å	$\bar{s}$ Å	$\bar{d}$ Å	ω/d	γ screw erg/cm^2	$\Delta\gamma$
Ti - 8.5 Al	22	390	520	280	20	170	2.3	9.9	0.5
Ti - 6.7 Al	9	430	480	290	50	250	1.7	9.0	1.1
Ti - 5.5 Al	7	350	400	280	-	169	2.1	10.8	-
Ti - 5.2 Al	12	320	490	160	-	154	2.1	11.7	-

However, it is apparent that the stacking fault energy does increase with decreasing aluminum concentration.

Tyson[14] predicted the preference of prism slip in Ti, Zr, and Hf, the stacking fault energies of which were anticipated to be high. A low basal plane stacking fault energy, such as observed in this study for Ti-8.5Al, should show a preference for basal slip, since dislocations dissociate to form two partial dislocations thereby restricting cross slip. Therefore, the preference of prism slip instead of basal slip with increasing aluminum concentration is certainly not obvious.

Curtis et al[15] has postulated that the occurrence of coplanar slip in α-titanium can result in decreased SCC because of two factors. First, coplanar slip can result in large normal stresses at the head of a dislocation pile-up. Second, the tendency toward preferential slip places additional constraints on the ability of the material at the tip of the crack to deform. Evidence has been shown that transgranular cracking in aqueous salt solutions in alpha and alpha-beta titanium alloys occurs predominately on or very near basal planes.[16] It would appear that the more dominant coplanar prism slip is most important during the initiation of the stress corrosion crack. Decreasing the basal plane stacking fault α-titanium with increasing aluminum would thus appear to be a more important factor during the crack propagation stage of the stress corrosion cracking process.

2.2 Effect of Stress and Temperature on Hydrogen Microsegregation and Embrittlement

At elevated temperatures, 500 to 650°F, where hot salt cracking is a problem, hydrogen diffusion does occur and plays a significant role in hot salt stress corrosion.[17] Gray[18] showed that embrittling effects of hot salt cracking on Ti-8Al-1Mo-1V could be removed by vacuum annealing.

It has been shown in this laboratory that hydrogen diffuses to titanium and precipitates at high stress regions at 600°F and 450°F[19] in titanium containing 500 ppm tritium. For beta-forged Ti-8Al-1Mo-1V containing 275 ppm tritium, an increasing concentration of tritium was observed with increasing stress at the alpha-beta interfaces at 600°F. Since commercial titanium alloys contain 50 to 150 ppm H_2 and additional hydrogen can be easily introduced by forming and processing operations, these results strongly suggest that hydrogen embrittlement could be a serious problem when localized stresses are present in elevated temperature applications.

Two possibilities that would explain the presence of large precipitates in pure titanium stressed in the temperature range 450°F to 600°F with the hydrogen content considerably below the solubility limit were considered:

A. The effect of pressure on the $\alpha/\alpha + \gamma$ phase boundary in Ti-H.

B. The effect of defect structure introduced by creep processes.

As far as could be determined, there are no data on the shift of the $\alpha/\alpha + \gamma$ phase boundary in the Ti-H system with pressure. However, there are extensive data on the effect of pressure on the $\gamma/\gamma + Fe_3C$ phase boundary in the Fe-C system. Because of the similarity of the α-titanium and γ-iron and the γ (TiH) and Fe_3C phases, it is felt that experimental results found for the Fe-C system could be applied to the Ti-H system to determine the approximate accuracy of thermodynamic calculations. Sufficient thermodynamic data were found in the literature for the Ti-H system to calculate the shift of the $\alpha/\alpha + \gamma$ phase boundary with pressure.

The α (Ti) and γ (Fe) phases are both close packed. The α (Ti) phase is hexagonal close pack and the γ (Fe) phase is face centered

cubic. Hydrogen has very little, if any, effect on the lattice parameter of α (Ti)[20] indicating little interaction between the hydrogen and titanium atoms. In the α lattice, these are two tetrahedral holes and one octahedral hole per titanium atom with the octahedral holes being the largest. The work of Hepworth and Schulmann[21] indicates that the hydrogen goes into the smaller tetrahedral holes.

In the case of carbon in gamma iron, the carbon atom most likely goes into the octahedral sites.[22] The phase diagrams are eutectic for the region of interest in both Ti-H and Fe-C.

Hilliard[23] has derived an expression describing the shift of the $\gamma/\gamma + Fe_3C$ boundary in the Fe-C system with pressure. It is given by:

$$RT\left[\frac{\partial \ell n C_\gamma}{\partial P}\right] T\left[\frac{1+\partial \ell n f_{C\gamma}}{\partial \ell n C_\gamma}\right] T, P = \frac{1-C_\gamma}{C_C - C_\gamma}\left[\frac{V_C}{4} - (1-C_C)\overline{V}_{Fe,\gamma} - C_C\overline{V}_{c,\gamma}\right] \quad (7)$$

Where the symbols and substituted values at 727° C are given below:

C_γ = atom fraction of C in γ; 0.0346
C_C = atom fraction of C in Fe_3C; 0.25
V_C = molar volume of Fe_3C; 23.92 cm^3
$\overline{V}_{Fe,\gamma}$ = partial molar volume of Fe in γ (Fe); 7.17 cm^3
$\overline{V}_{c,\gamma}$ = partial molar volume of C in γ (Fe); 4.47 cm^3
R = gas constant; 0.0831 cm^3 Kb/mol K

$$\left[\frac{1 + \partial \ell n f_{c,\gamma}}{\partial P}\right] = 1.28$$

where $f_{c,\gamma}$ is the activity coefficient of C in γ(Fe).

For these values

$$\left[\frac{\partial \log C_\gamma}{\partial P}\right] T = -9.5 \times 10^{-3}\ Kb^{-1}$$

at 727° C. Hilliard obtained experimental values of the change in C_γ with respect to pressure and the comparison is shown in Figure 7. In the region of 0 to 10 Kb, Equation (4) predicts reasonably well the variation of C_γ with pressure.

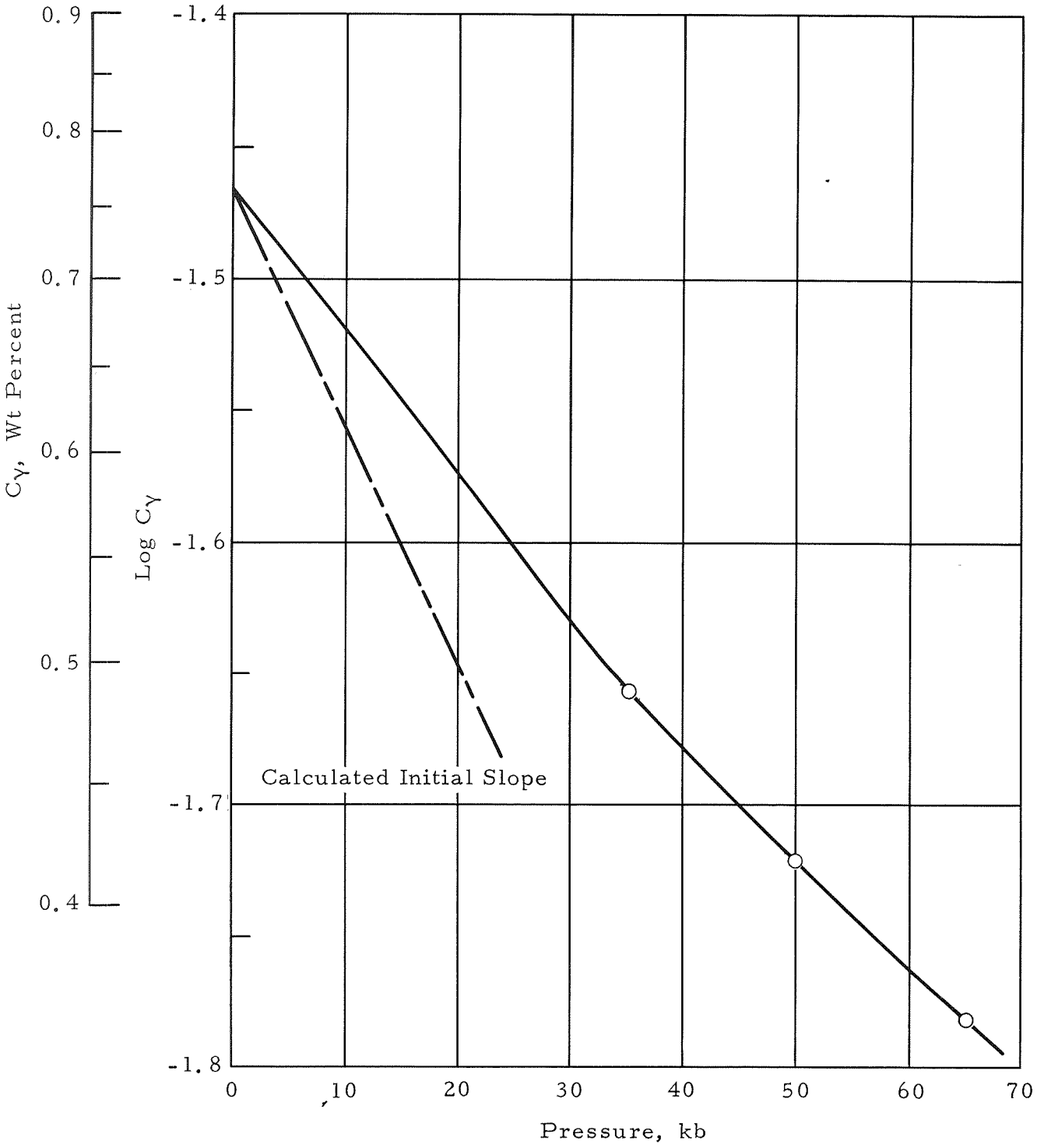

Figure 7. Plot of Log C_γ versus Pressure Where C_γ is Atomic Fraction of Carbon in Austenite in Equilibrium with Fe_3C at 727°C. The initial slope of the curve was computed from Eq. (7)[23]

Nilan[24] has shown that the phases and microstructures produced in Fe-C alloys by isothermal transformation could be explained entirely by the shift of the diagram with pressure. That is, no phases were produced and no microstructures were produced at high pressure that are not found at atmospheric pressure. The only difference is that the entectoid point is shifted.

These experiments suggest that in the Ti-H system, no phases or microstructures should be formed under pressure that are not formed at atmospheric pressure. Further, the shift of the $\alpha(\alpha+\gamma)$ phase boundary can be calculated from thermodynamic properties and should be reasonably close to the actual shift.

Since Equation (7) is applicable for equilibrium conditions, it can be written in the following form for the Ti-H system:

$$RT\left[\frac{\partial \ell n C_H^{\alpha}}{\partial P}\right]\left[\frac{1+\partial \ell n f_{H,\alpha}}{\partial \ell n C_H^{\alpha}}\right] = \frac{1 - C_H^{\alpha}}{C_H^{\alpha} - C_H^{\alpha}}\left[0.47V_{\gamma} - \left(1 - C_H^{\gamma}\right)\overline{V}_{Ti,\alpha} - C_H^{\gamma}\overline{V}_{H,\alpha}\right] \quad (8)$$

The following values were substituted in Equation (8) at the experimental temperatures of 600°F and 450°F.

C_H^{α} = atom fraction of hydrogen in α at the $\alpha/\alpha+\gamma$ boundary 0.06 at 600°F and 0.031 at 450°F.[22, 26]

C_H^{γ} = atom fraction of hydrogen in γ at the $(\alpha+\gamma)$ boundary. Gibb and Kruschwitz[27] reported that γ with lattice parameter of 4.395 Å contains 0.463 atom fraction of hydrogen, whereas, Haag[28] reported a lattice parameter of 4.397 Å with 0.488 atom fraction of hydrogen. An average value of 0.47 atom fraction was used in these calculations. Since there are no data on the $\gamma/\alpha+\gamma$ boundary as it changes with temperature, it is assumed that it is constant.

$\left[\frac{\partial \ell n f_{H,\alpha}}{\partial \ell n C_H^{\alpha}}\right]_{T,P}$ = rate of change of the activity coefficient with hydrogen concentration = 0

At 450°F and 600°F McQuillan[20] and Hepworth and Schulmann[21] have shown that for the α phase, the concentration of hydrogen is linearly proportional to $\sqrt{p}$. From this, it is apparent that the activity coefficient is independent of concentration.

V_γ = molar volume of γ=12.984 cm^3 at 600°F and 12.953 cm^3 at 450°F. The phase is fcc with lattice parameter 4.396 kx. This is the room temperature parameter for γ in an $\alpha+\gamma$ mixture. If it is assumed that the volume coefficient of thermal expansion for γ is the same as that for α, the unit cell volume calculated at 450°F and 600°F is 86.065 A^3 and 86.270 A^3. From these unit cell volumes, the molar volume can be calculated since there are 4 molecules/unit cell. Although this assumption may not be a valid assumption, it should not introduce a significant error in the calculation of the molar volume.

$\bar{V}_{Ti,\alpha}$ = partial molar volume of Ti in α=10.270 cm^3 at 600°F, 10.690 cm^3 at 450°F. Pearson[28] gives the lattice dimensions of α at room temperature as a=2.943 c=4.6728 kx and at 576°F as a=2.952 c=4.690. Grenier and Ellis[29] showed the thermal expansion to be linear between 30 and 200°C. Assuming a linear coefficient of expansion, the lattice parameters for α-titanium are a=2.958 A and c=4.700 A at 600°F and a=2.956 A and c=4.695 A at 450°F.

$\bar{V}_{H,\alpha}$ = partial molar volume of H in α-titanium = 0.620 cm^3 at 600°F and 0.242 cm^3 at 450°F. McQuillan[20] reported that the lattice parameters of α are independent of hydrogen content throughout the solubility range. This result along with the values of C_H^α reported above were used to calculate $V_{H,\alpha}$.

Substituting the above values in Equation (8), the

$$\frac{\partial \log C_H^\alpha}{\partial P} = 2.63 \times 10^{-3}\ Kb^{-1} \text{ at } 600°F$$

$$\frac{\partial \log C_H^\alpha}{\partial P} = 7.35 \times 10^{-3}\ Kb \text{ at } 450°F.$$

In both cases, the solubility of hydrogen in α-titanium increases with pressure.

From the thermodynamic calculation, 10 Kb should increase the solubility of hydrogen in alpha from 0.06 to 0.064 and from 0.031 to 0.037 atom fraction at 450°F. If a triaxial state equal to the yield stress is assumed, then a pressure of only about 1 Kb can be realized in pure α-titanium. The shift in the solubility equilibrium curve would, therefore, be considerably less than these values.

These results clearly indicate that the large gamma hydride precipitates observed in α-titanium, stressed at 450°F and 600°F, did not occur during the stressing cycle because of a shift in the solubility equilibrium curve.

If the gamma hydride precipitates are not formed during the stressing cycle, they must, therefore, form during the quenching cycle. Since the unstressed α- titanium showed only fine precipitates when rapidly quenched, it seems logical to assume that the large precipitates form during quenching at defect sites which are introduced into α- titanium during the stressing cycle.

In the deformation of unalloyed titanium, a number of slip and twinning systems have been observed. At room temperature, both slip and twinning systems are active. Slip occurs on the $\{0001\}\langle 11\bar{2}0\rangle$, $\{10\bar{1}0\}\langle 11\bar{2}0\rangle$, and $\{10\bar{1}1\}\langle 11\bar{2}0\rangle$.[30,31,32] Increasing temperature tends to favor slip. It has been shown by Jones, et al.[33] that the primary slip system of α-titanium in the temperature range of ambient to 800°F is $\{10\bar{1}0\}\langle 10\bar{1}0\rangle$.

An X-ray examination of large grain size α-titanium shown in Figure 7 identified that the primary habit plane for gamma hydride precipitates is $\{10\bar{1}0\}$. The angles between hydride platelets in micro-autoradiographs shown previously,[19] were 60°, indicating that the prism planes are the habit planes for gamma hydride precipitation.

Since tapered rod specimens were used in these experiments, it was not possible to measure the creep rate during the stressing cycle. However, it seems logical to assume that the dislocations generated during the stressing cycle on $\{10\bar{1}0\}$ prism planes serve as nucleating sites for gamma hydride precipitation during the quenching cycle.

REFERENCES

1. T.L. Mackay and N.A. Tiner, "Stress Corrosion Susceptibility of Titanium Alloys in Aqueous Environments," Metals Eng. Quart., 9, pp. 59-60 (1969).

2. W.F. Brown and J.R. Srawley, "Plane-Strain Crack Toughness Testing of High Strength Metallic Materials," ASTM STP 410 (1966).

3. M.J. Blackburn and J.C. Williams, Trans. Am. Soc. Metals, 62, pp. 398-409 (1969).

4. P.C.J. Gallagher and Y.C. Lin, Acta. Met. 17 p. 127 (1969).

5. L.M. Brown and A.R. Tholen, Disc.Faraday Soc. 38 p. 35 (1966).

6. R. Siems, Disc. Faraday Soc. 38 p. 42 (1964).

7. T. Jossang, M.J. Stowell, J.P. Hirth and J. Lothe, Acta. Met. 13 p. 279 (1965).

8. P.C.J. Gallagher, J. Appl. Phys. 37, p. 1710 (1966).

9. T. Ericsson, Acta. Met. 14 p. 853 (1966).

10. K.H.G. Ashbee and L.F. Vassamillet, Acta. Met. 15, p. 481 (1967).

11. A.W. Ruff and L.K. Ives, Acta. Met. 17, p. 1045 (1969).

12. M.J. Whelan, J. Inst. Metals 87, p. 392 (1958).

13. W.B. Pearson, A Handbook of Lattice Spacings and Structures of Metals and Alloys, Pergamon Press, p. 599 (1964).

14. W.R. Tyson. "Basal and Prismatic Slip in hep Crystals," Acta. Met, 15 p. 574 (1967).

15. R.E. Curtis, R.R. Boyer and J.C. Williams, Trans. Am. Soc. Metals, 51, pp. 115-127 (1968).

16. D.N. Fager and W.F. Spurr, ASM Trans. Quarterly 61, pp. 283-391 (1967).

17. D. N. Williams, "Basic Mechanisms of Stress Corrosion Cracking of Titanium," Stress Corrosion Cracking of Titanium, Spec. Tech. Publ. No. 397, ASTM, pp. 137-151 (1966).

18. H.R. Gray, "Hot Salt Stress-Corrosion of Titanium Alloys: Generation of Hydrogen and its Embrittling Effects," NASA TN D-5000 (1969).

19. T.L. Mackay, "Stress Corrosion Cracking of Titanium Alloys at Ambient Temperature in Aqueous Solutions," NASA CR-1464 (1969).

20. A. B. McQuillan, Proc. Royal Soc. (London) Ser. A. 204, p. 309, (1950).

21. M. T. Hepworth and R. Schulmann, Jr., Trans. A. I. M. E., 224, p. 928 (1962).

22. J. S. Peters, J. I. S. I. 145, p. 111 (1942).

23. J. E. Hilliard, Trans. A. I. M. E. 227, p. 429 (1963).

24. T. G. Nilan, Trans. A. I. M. E. 239, p. 898 (1967).

25. G. A. Lenning, C. M. Craighead and R. I. Jaffee, "Constitutional and Mechanical Properties of Titanium-Hydrogen Alloys," Trans. A. I. M. E., 200, p. 367 (1954).

26. W. L. Koster, L. Bangert and M. Evans, "Damping Behavior of Hydrogen-Loaded Titanium," Z. Metalkunde, 47, p. 564 (1956).

27. T. R. Gibb and H. W. Kruschwitz, J. Am. Chem. Soc. 72, p. 5365 (1950).

28. W. B. Pearson, A Handbook of Lattice Spacings and Structure of Metals and Alloys, Pergamon Press p. 873 (1964).

29. E. S. Grenier and W. S. Ellis, Trans. A. I. M. E. 80, p. 657 (1949).

30. F. C. Rossi, C. A. Dube, and B. H. Alexander, "Mechanism of Plastic Flow in Titanium Determination of Slip and Twinning Modes," Trans. A. I. M. E., 197, p. 657 (1953).

31. E. A. Anderson, D. C. Jillson, and J. R. Dunbar, "Deformation Mechanisms in Alpha-Titanium," Trans. A. I. M. E., 197, p. 1191 (1953).

32. A. T. Churchman, "The Slip Modes of Titanium and the Effect of Purity on Their Occurrence During Tensile Deformation of Single Crystals," Proc Roy Soc 226A, p. 257 (1953).

33. R. L. Jones, F. W. Cooke, H. Conrad, and B. R. Banerjee, "Investigations to Understand the Deformation and Strengthening Mechanisms of the Solid Solution Phases of Titanium," AFML-TR-68-28 (1968).